UC SANTA BARBARA
engineering

Igor Mezic,
Mechanical Engineering,
UC Santa Barbara

Report on ONR-MURI Work in 2010-2013

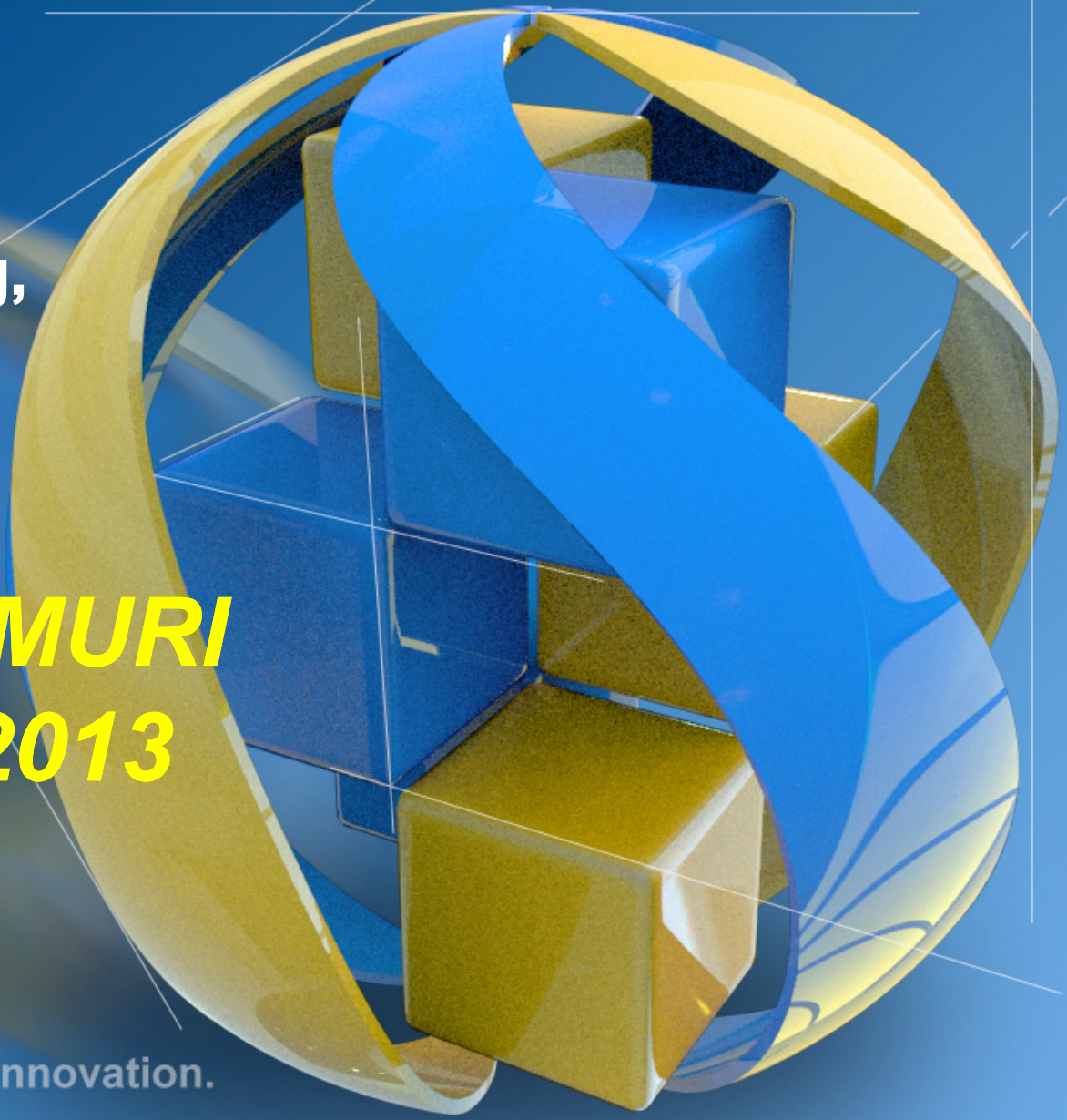

The convergence of research and innovation.

A versatile experimental testbed for 3D+1 mixing characterization.

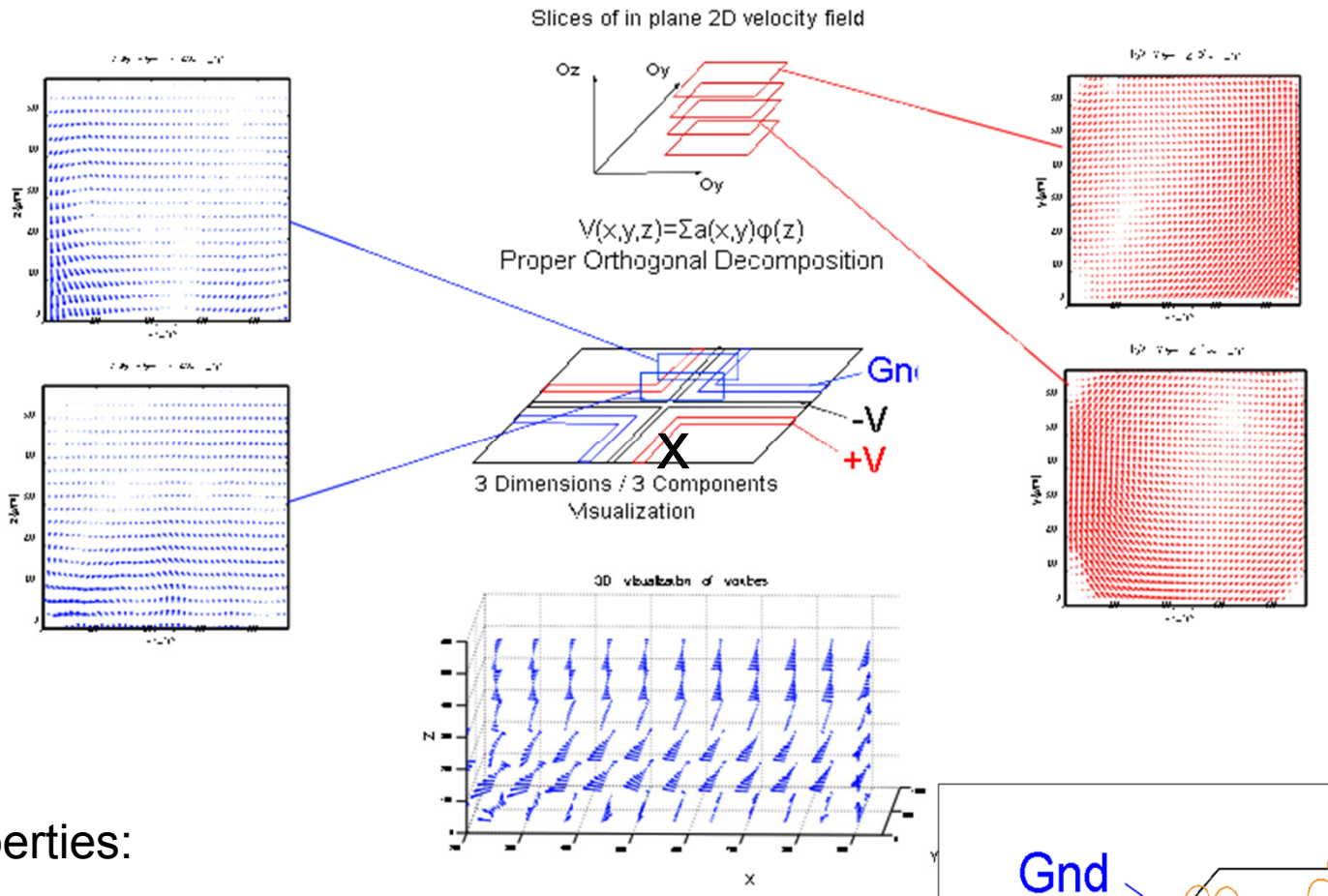

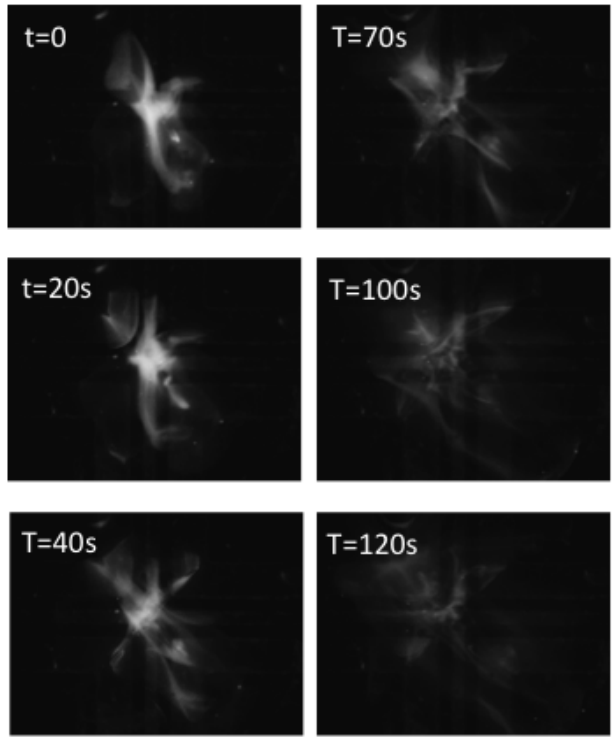

Top Views of 1µm bead mixing over time

Properties:

-Ability to emulate physical forces with arbitrary dependence on time.

-Full PIV-based characterization of 3D+1velocity field enable linkage with theoretical progress on visualization of 3-D structures (see next slide).

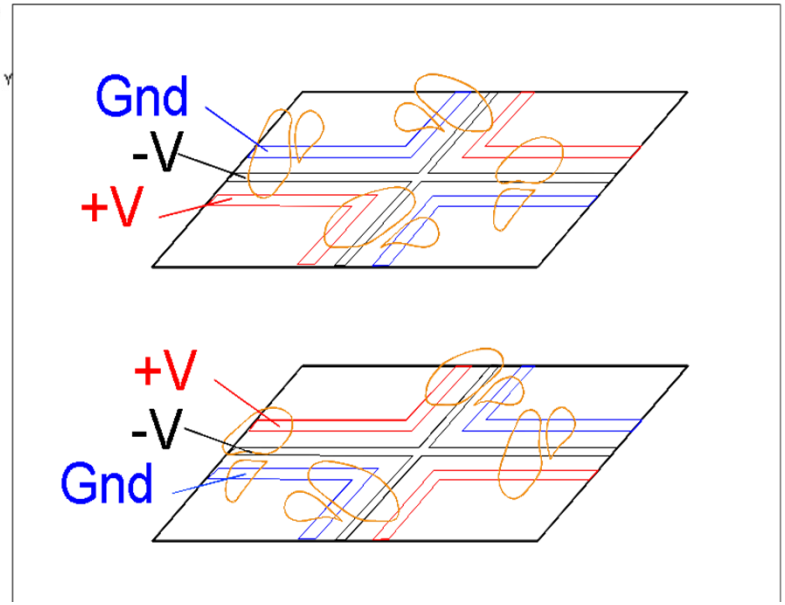

Side View

Ergodic Quotient

$$x \xrightarrow{\Phi} \mu_x$$

$$\frac{1}{N}\sum_{n=0}^{N-1} f \circ T^n(x) \xrightarrow[N\to\infty]{\text{weak-}*} \int f d\mu_x$$

Each initial condition has an ergodic empirical measure associated to it.

$$\tilde{f}(x) = \frac{1}{N}\sum_{n=0}^{N-1} f \circ T^n(x)$$

$$f_k(x) = e^{i2\pi(k\cdot x)}, \quad k \in \mathbb{Z}^d$$

By averaging a basis of continuous functions on the state space manifold, we can represent empirical measures in a weak sense.

$$x \xrightarrow{\Phi} [\ldots, \tilde{f}_k(x), \ldots] \subset l_\infty(\mathbb{Z}^d)$$

We obtain representation of ergodic measures in a sequence space.

Theorem. (Discrete topology) Ergodic quotient map separates the ergodic partition, i.e., points x and y are in the same ergodic set iff

$$\Phi(x) = \Phi(y)$$

Ergodic partition is equivalent to the quotient of the state space by level sets of all time-averaged functions

Metric Geometry

Ergodic Quotient

$$\xi = \{\Phi(x) : x \in \mathcal{M}\} \subset l_\infty$$

$$\|\mu_x - \mu_y\|^2 = \sum_{k \in \mathbb{Z}^d} \frac{\left|\tilde{f}(x) - \tilde{f}(y)\right|^2}{[1 + (2\pi \|k\|)_2]^s}$$

Endow the ambient space with a weighted Euclidean metric that corresponds to negative-index Sobolev space of containing invariant measures.

What can geometry of the ergodic quotient tell us about corresponding state space structures?

State space

Ergodic Quotient

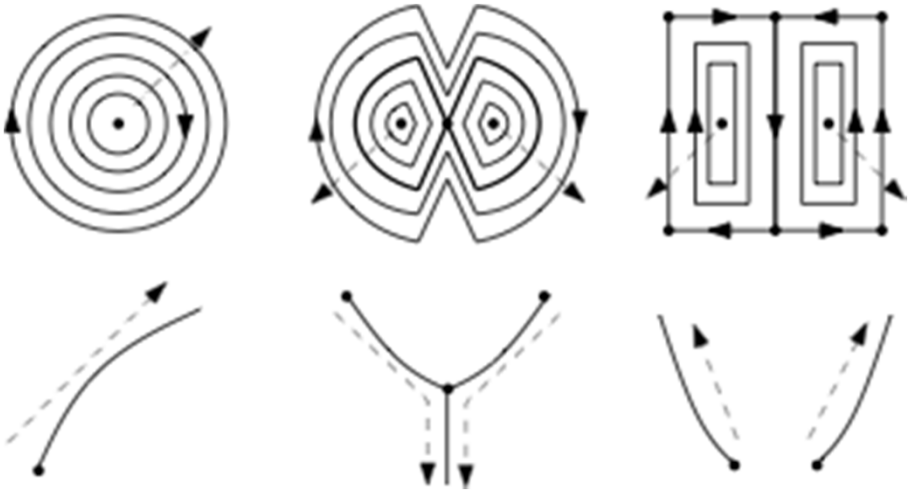

Sufficiently many local integrals of motion imply local continuity of the ergodic quotient (can be formulated rigorously).

Computational Geometric Analysis

Goal: detect locally connected subsets of EQ to identify trajectories that lie within a regions with local integrals of motion.

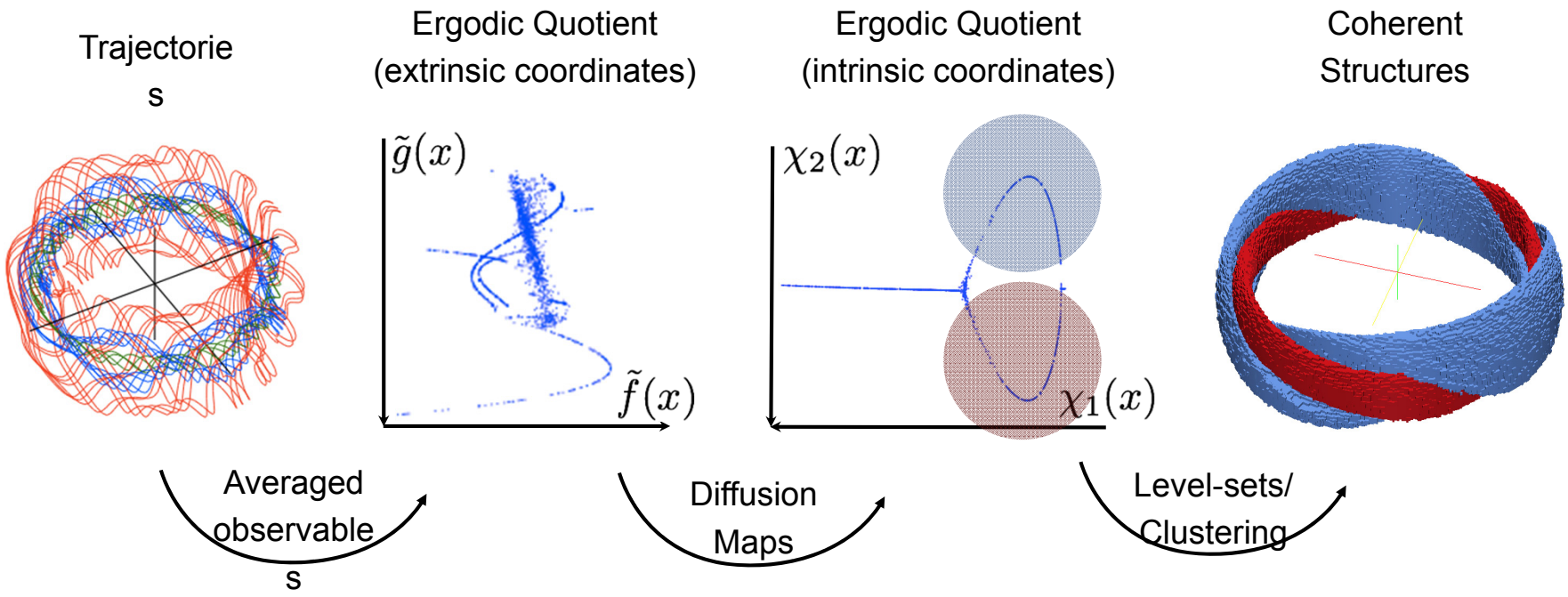

Compute numerical diffusion modes on the ergodic quotient to obtain low-dimensional representation of the ergodic quotient.

Geometric clustering, e.g., *k*-means, in diffusion space can then extract connected subsets. Color trajectories based on the membership in clusters.

ABC flow: Global Structure

$$\begin{bmatrix}\dot{x}\\ \dot{y}\\ \dot{z}\end{bmatrix} = \begin{bmatrix}A\sin z + C\cos y\\ B\sin x + A\cos z\\ C\sin y + B\cos x\end{bmatrix} \qquad A=\sqrt{3}, B=\sqrt{2}, C=1$$

State space clusters

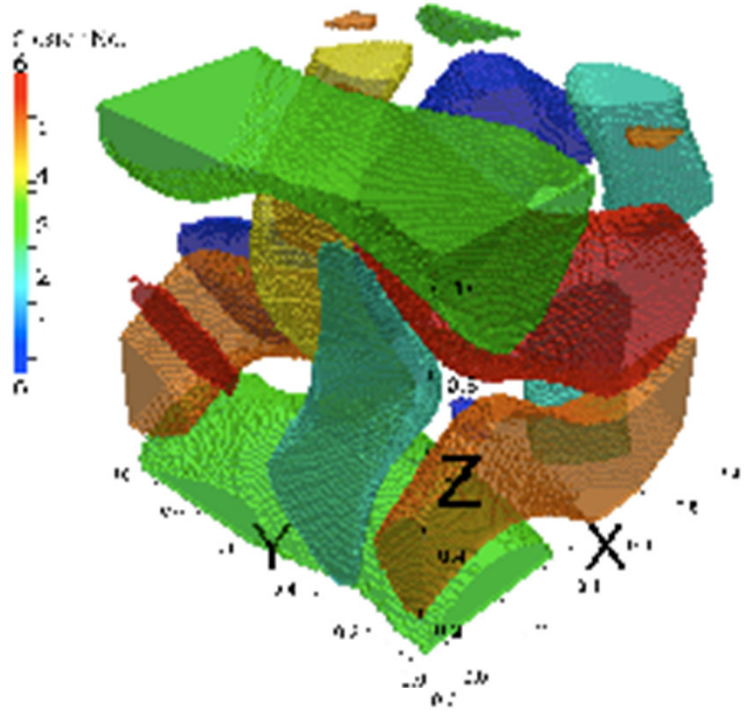

(a) Six subsets in the state space corresponding to six clusters of aggregation. Subsets contain primary vortices of the ABC flow. The chaotic sea between vortices is the seventh cluster and appears as the void between vortices.

Ergodic Quotient

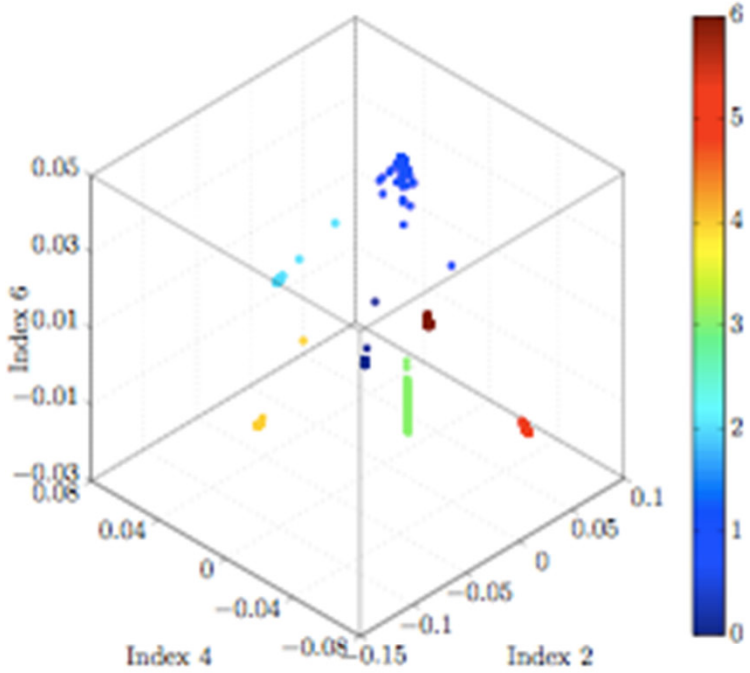

(b) Projection of ergodic quotient onto three out of ten diffusion coordinates used for clustering. Points were colored according to membership in clusters. The central cluster corresponds to the chaotic sea.

FIG. 2: Six primary vortices extracted by k-means clustering ($k = 7$) of projection of ergodic quotient onto first 10 diffusion coordinate. ABC flow (10) was simulated with $A = \sqrt{3}$, $B = \sqrt{2}$, $C = 1$, from $N = 1000$ initial conditions uniformly distributed in basic periodicity cell $[0, 1)^3$, with observables cut off at wavenumber $K = 10$, and convergence tolerance ATOL $= 2 \times 10^{-4}$.

ABC Flow: Comparison

Theory:

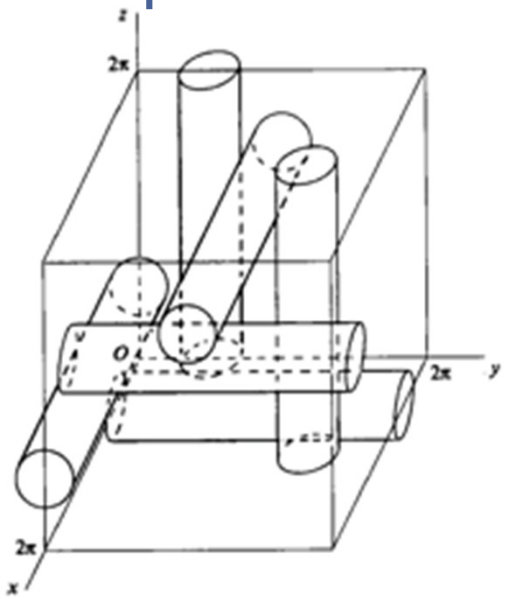

[Dombre et al.,1986]

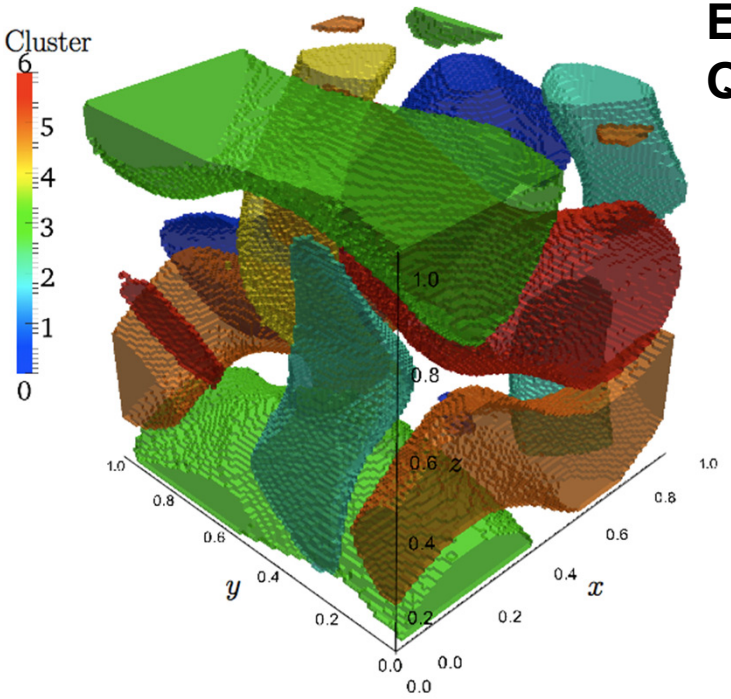

Ergodic Quotient

Finite-Time Lyapunov Exp.

Ulam's Method

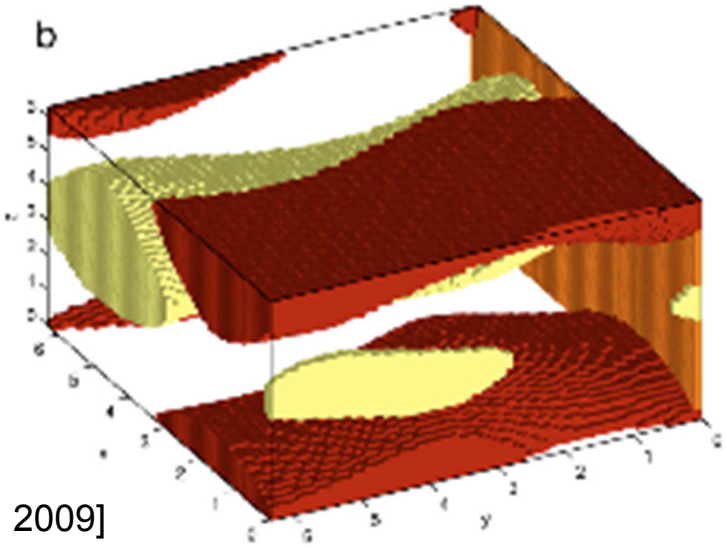

[Froyland, Padberg, 2009]

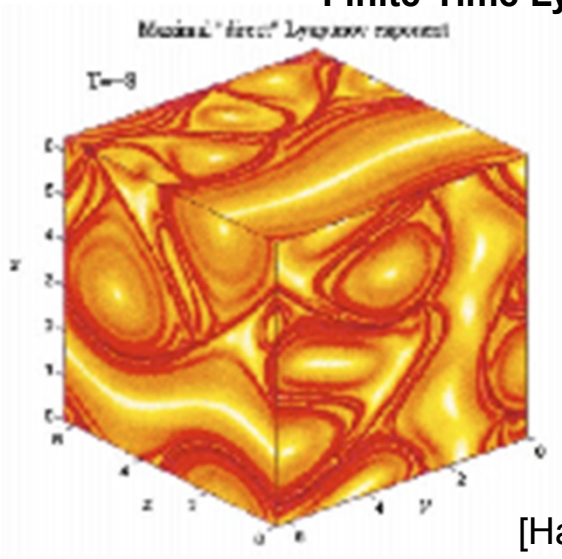

[Haller, 2001]

System: Fluid-like, 3D+time flow

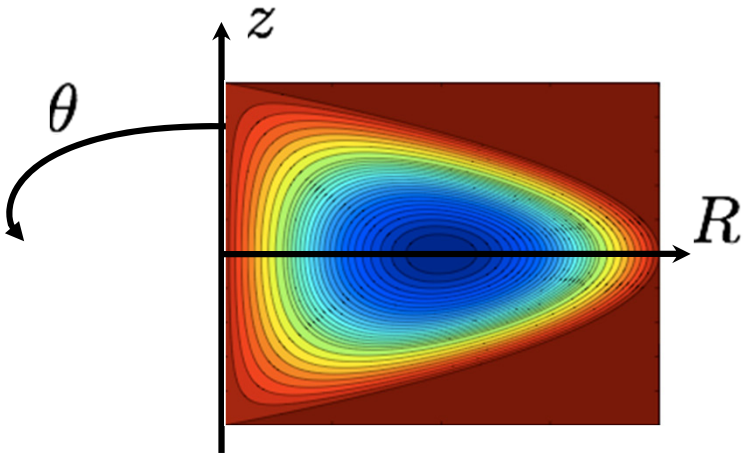

Hill's Vortex

Perturbation

$$\begin{bmatrix} \dot{R} \\ \dot{z} \\ \dot{\theta} \end{bmatrix} = \begin{bmatrix} 2Rz \\ 1-4R-z^2 \\ \frac{c}{2R} \end{bmatrix} + \varepsilon \begin{bmatrix} \sqrt{2R}\sin\theta \\ \frac{z}{\sqrt{2R}}\sin\theta \\ 2\cos\theta \end{bmatrix} \sin 2\pi t$$

Swirl

$$(R, z, \theta) \in \mathbb{R}^+ \times \mathbb{R} \times \mathbb{T}$$

- Unperturbed: Hamiltonian at each slice $\theta = const.$
- Volume preserving swirl and perturbation
- KAM behavior at small $c = \varepsilon$

Invariant sets (using EQ)

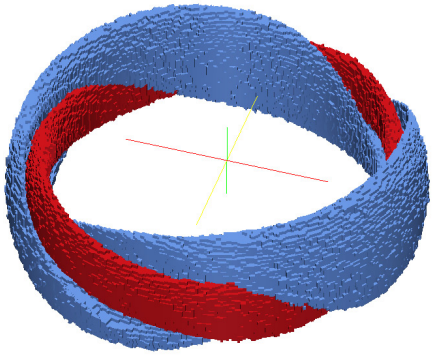

Canonical coordinates

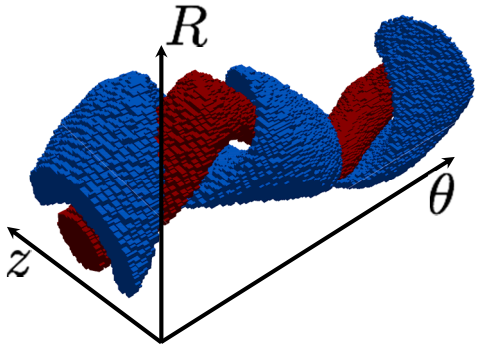

Angle unraveled

Two elliptic regions exist.
- Red, leftover from unperturbed elliptic region;
- Blue, borne out of separatrix for unperturbed case.

Bifurcation uncovered using ergodic quotient

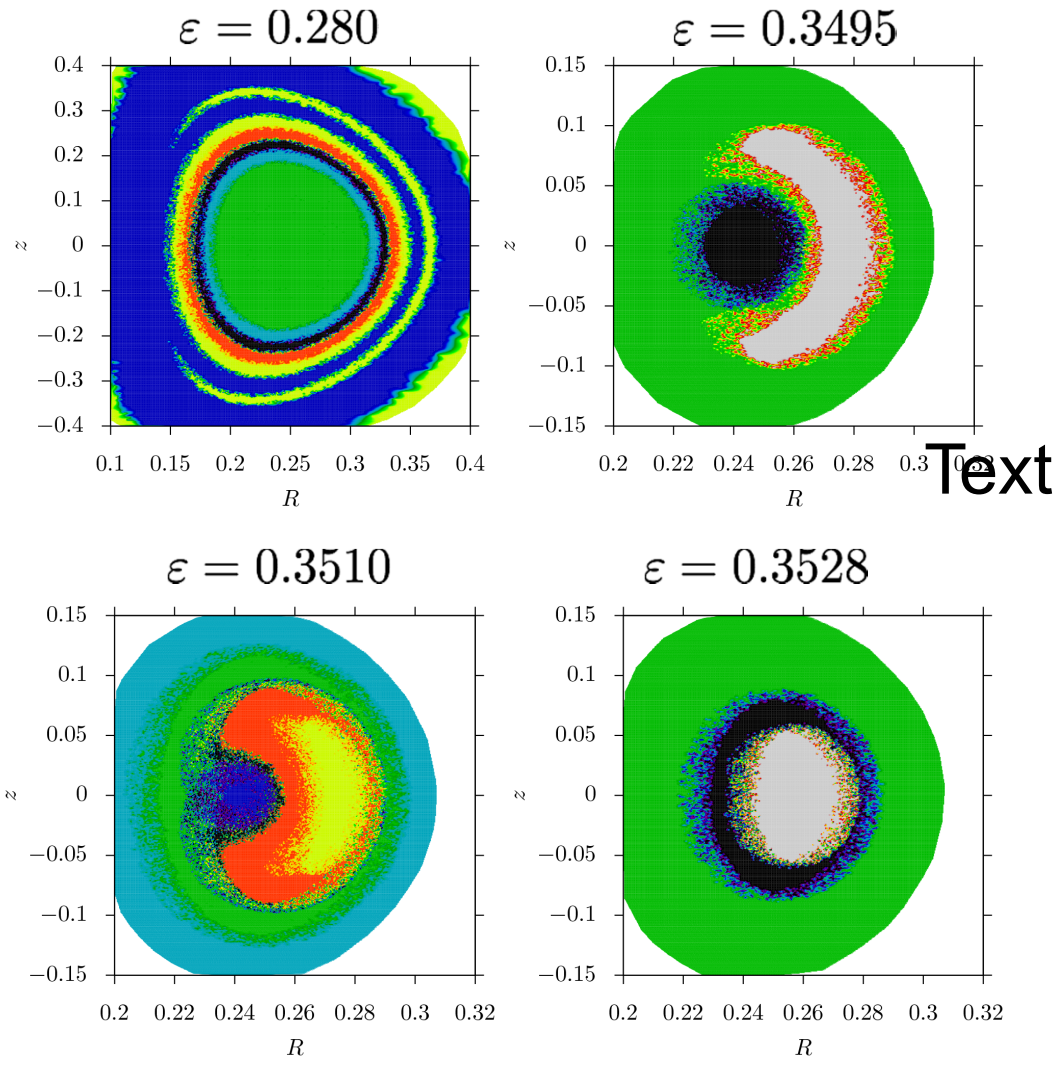

Text

The winding elliptic region replaces the central elliptic region at the center of the state space.

Conclusions:

- **Ergodic quotient is useful** for discovering unknown features
- **New bifurcation uncovered**, seemingly consistent with a saddle-node collision mechanism for periodic sets
- Similar phenomenon seen in 1:2 resonances for Hamiltonian systems, e.g., spring-pendulum oscillator [Broer ' 03]

Mesohyperbolicity in 2D

Notation:

- $\phi_{t_0}^{t+T}(\mathbf{x}_0)$: the map of A mapping the fluid particle starting at time t_0 at point $\mathbf{x}_0 \in \mathbb{R}$ to its position $\mathbf{x}$ at time $t_0 + T$.
- $D\phi_{t_0}^{t+T}(\mathbf{x}_0)$ is the Jacobian matrix $J(\mathbf{x}_0) = \partial\mathbf{x}/\partial\mathbf{x}_0$.

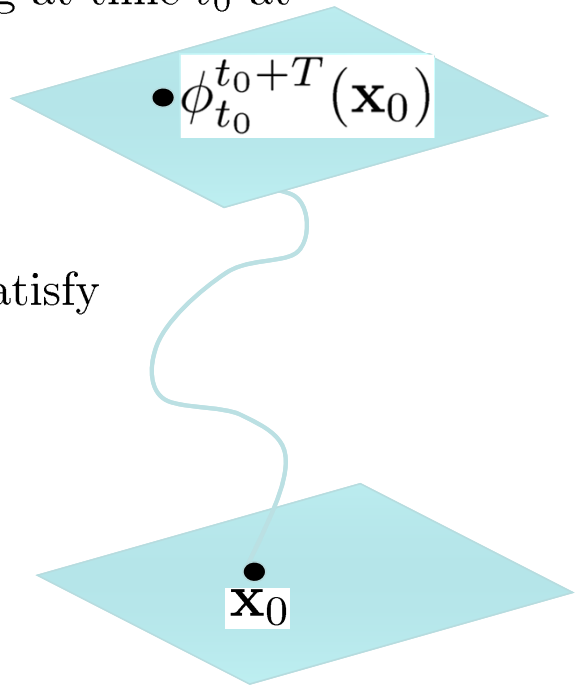

Note:

$\mathbf{v}$ is volume-preserving so the eigenvalues $\lambda_{1,2}(\mathbf{x}_0)$ of $J(\mathbf{x}_0)$ satisfy

$$\det(J(\mathbf{x}_0)) = \lambda_1(\mathbf{x}_0)\lambda_2(\mathbf{x}_0) = 1.$$

Thus, they are either real and

$$\lambda_1(\mathbf{x}_0) = 1/\lambda_2(\mathbf{x}_0)$$

or complex conjugate on the unit circle,

$$|\lambda_{1,2}(\mathbf{x}_0)| = 1.$$

A trajectory starting at $\mathbf{x}_0$ is

mesohyperbolic if $\lambda_{1,2}(\mathbf{x}_0)$ are real and

mesoelliptic if the eigenvalues are complex conjugate.

Mesohyperbolicity in 2D

Theorem A trajectory is mesohyperbolic on interval $[t_0, t_0 + T]$ provided

$$(T^2 \det \nabla \mathbf{v}^*(\mathbf{x}_0, t_0, T) - 4) \det \nabla \mathbf{v}^*(\mathbf{x}_0, t_0, T) > 0$$

and mesoelliptic if

$$(T^2 \det \nabla \mathbf{v}^*(\mathbf{x}_0, t_0, T) - 4) \det \nabla \mathbf{v}^*(\mathbf{x}_0, t_0, T) < 0$$

.

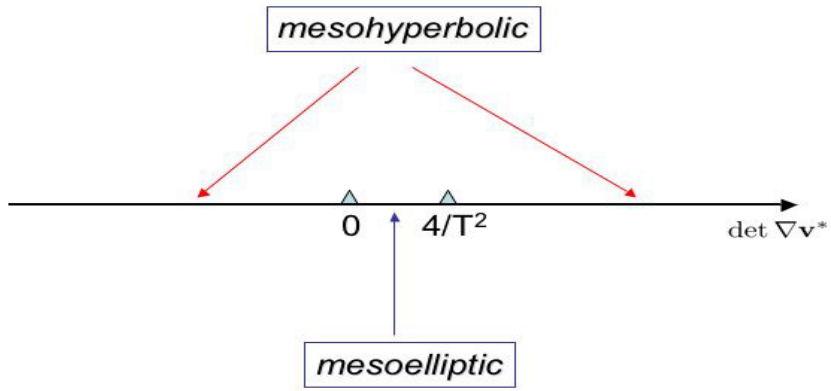

Flow Structures in 2D

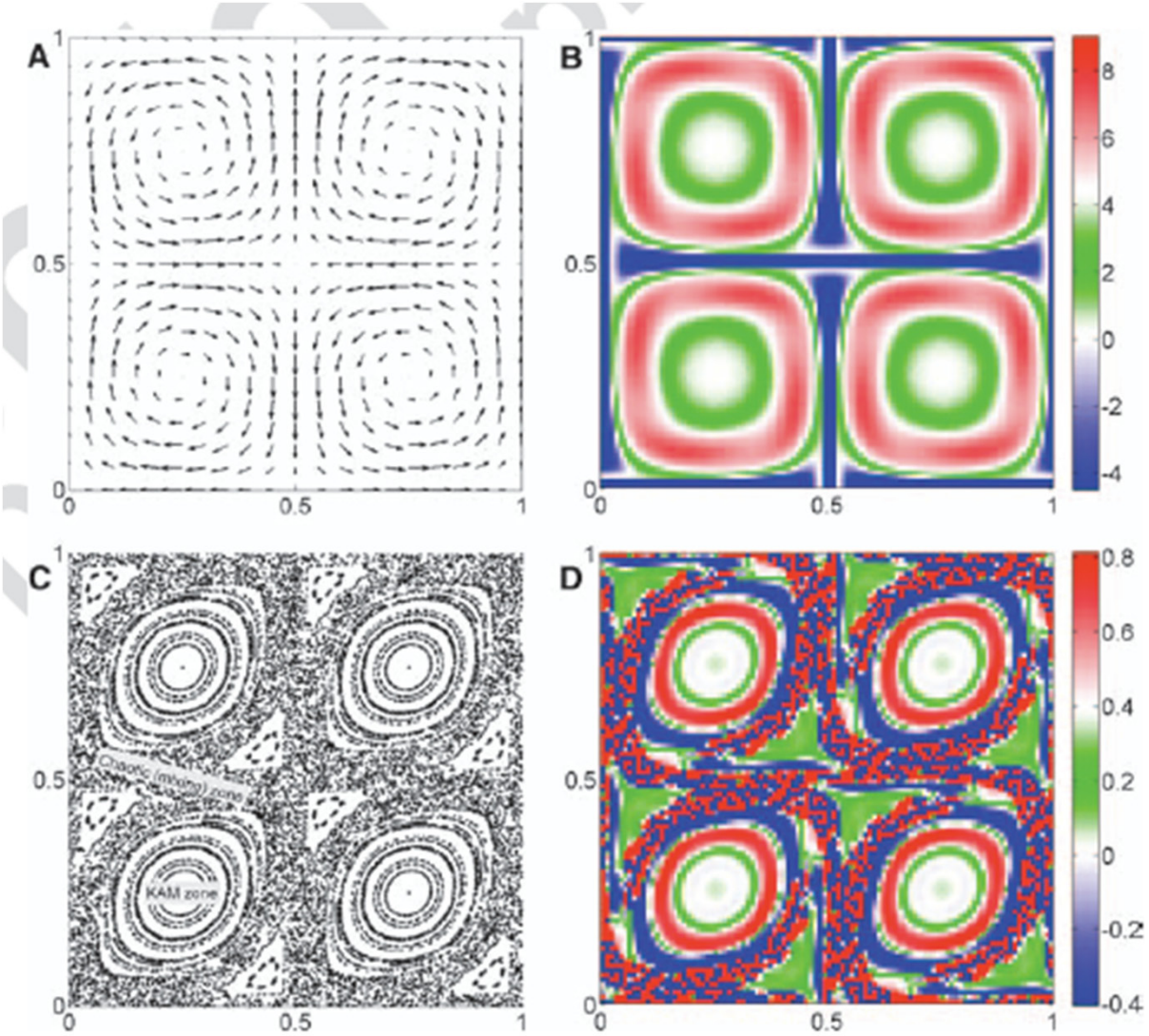

Fig. 1. (**A**) A cellular, divergence-free velocity field described in Eq. 6. (**B**) Hypergraph map for the velocity field shown in (A), for $T = 0.94248$. (**C**) Poincaré map for the time-periodic, divergence-free perturbation of the velocity field shown in (A) by a vector field described in Eq. 7, with $\epsilon = 0.1$. (**D**) Hypergraph map for the time-periodic velocity field whose Poincaré map is shown in (C), for $T = \pi$.

I.M., S. Loire,
V. Fonoberov, P. Hogan, ***Science*** *(2010)*

Gulf Oil Spill Prediction

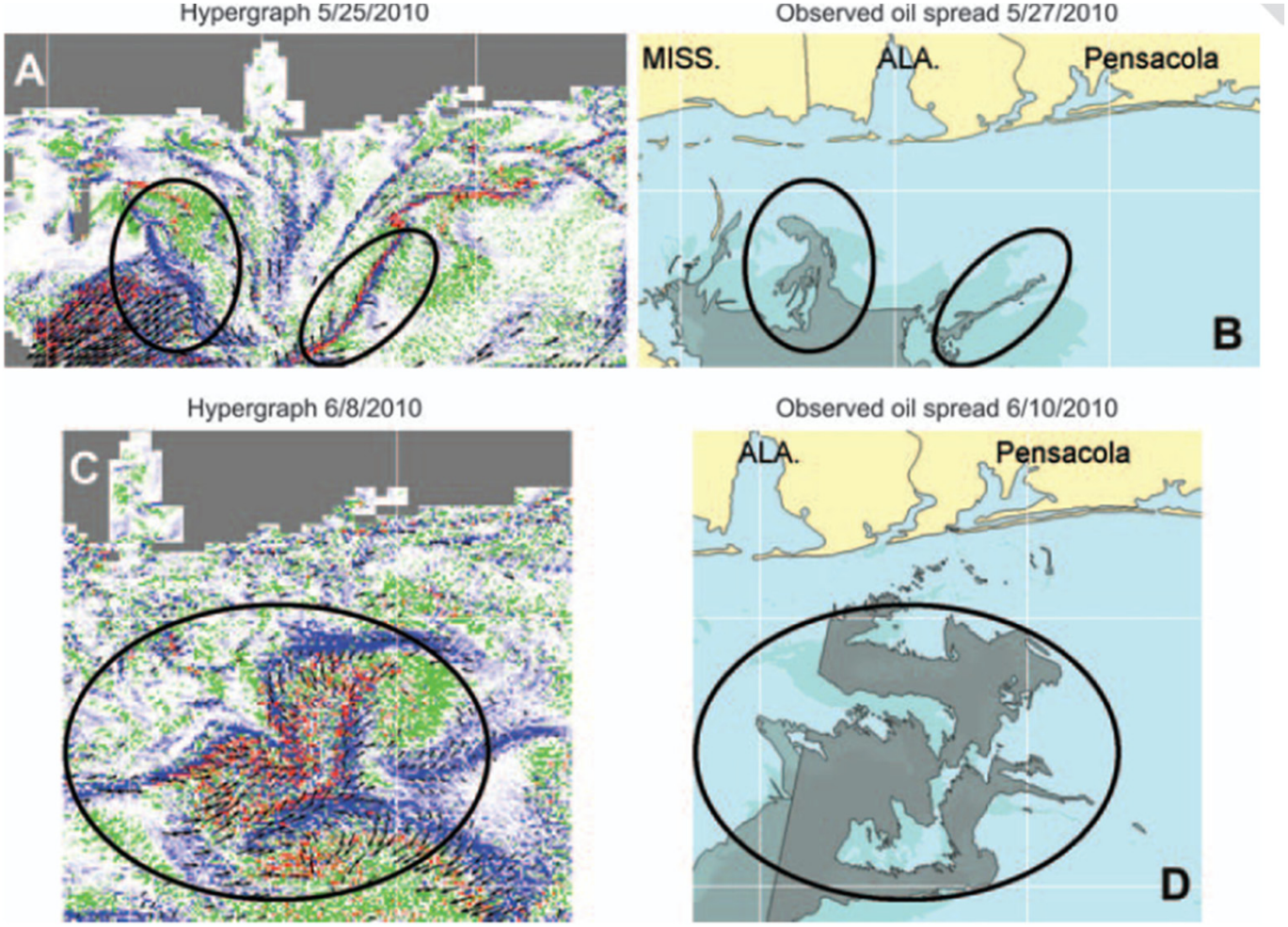

Fig. 3. (**A**) Ocean hypergraph map in front of the Biloxi-Pensacola shoreline on 25 May, forecasting strong oil incursion toward the coastline (circled) in the following 3 days. (**B**) NOAA's oil spread estimate in front of the Biloxi-Pensacola shoreline on 27 May. The major directions of oil spread were predicted by the hypergraph map 2 days earlier. The oil reached the shore several days later, on 2 June. (**C**) Ocean hypergraph map in front of Pensacola on 8 June, forecasting a strong oil mixing event in front of the shoreline and extension of the oil slick toward Panama City Beach in the following 3 days. (**D**) NOAA's oil spread estimate on 10 June in front of Pensacola. The oil developed a large slick forecasted by the hypergraph map 2 days earlier and continued to flow toward Panama City Beach.

Analysis based on

$$\det \nabla \mathbf{v}^*(\mathbf{x}_0)$$

In 2-D AND 3-D

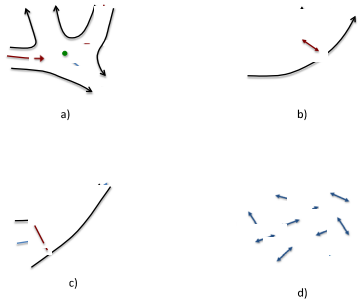

Robust, hyperbolic behavior

I.M., S. Loire, V. Fonoberov, P. Hogan, ***Science*** *(2011)*

Finite-time flow map of a (nonautonomous) vector field $\dot{x} = f(t,x),\ x \in \mathbb{R}^D$

Flow map

Mesochronic vector field

$$\Phi_{t_0}^{t_0+T}(x) = x + T \cdot \underbrace{\frac{1}{T}\int_{t_0}^{t_0+T} f\left[\tau, \Phi_{t_0}^{\tau}(x)\right] d\tau}_{\tilde{f}_T(x)}$$

Hyperbolicity of the flow map can be inferred from the eigenvalues/characteristic polynomial of Jacobian of mesochronic vector field.

We are interested in capturing locations of eigenvalues of the flow map, not necessarily its eigenvectors.

Mesohyperbolicity for 3d incompressible flows

Real valued spectral characteristics of the Jacobian, evaluated without computing eigenvalues.

$$t_{\tilde{f}}(x) = \mathrm{tr}[\nabla \tilde{f}_T](x) = \sum_i \lambda_i(x),$$
$$m_{\tilde{f}}(x) = \mathrm{tr}\,\mathrm{Adj}[\nabla \tilde{f}_T](x) = \sum_i \prod_{j\neq i} \lambda_j(x),$$
$$d_{\tilde{f}}(x) = \det[\nabla \tilde{f}_T](x) = \prod_i \lambda_i(x)$$

Incompressibility constraint: $t_{\tilde{f}} + T m_{\tilde{f}} + T^2 d_{\tilde{f}} \equiv 0$

Mesohyperbolicity conditions:

$$\mathcal{C}_+ := d_{\tilde{f}} \neq 0$$
$$\mathcal{C}_- := 3T^3 d_{\tilde{f}} + 2T^2 m_{\tilde{f}} - 8 \neq 0$$

Two quantities determine the **character** of the mesohyperbolic behavior:

$$\Sigma\left(d_{\tilde{f}}(x), m_{\tilde{f}}(x), T\right)$$

Rational function.
Sign determines **flattening/elongating** character of flow map over interval T at point x.

$$\Delta\left(d_{\tilde{f}}(x), m_{\tilde{f}}(x), T\right)$$

Polynomial function.
Sign determines rotation: **focal/nodal** character of flow map over interval T at point x.

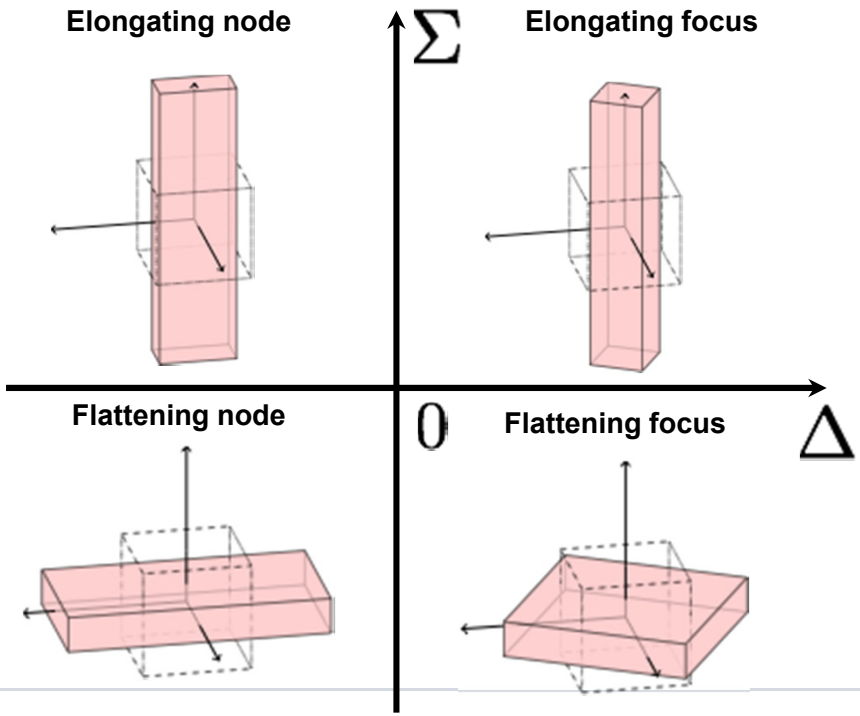

Computing the mesochronic Jacobian

Time-evolution method

1. Integrate the trajectory

$$t \mapsto \Phi_{t_0}^t, \ \forall t \in [t_0, t_0 + T]$$

2. Evaluate the instantaneous Jacobian

$$J_p(t) = (\nabla f)\left[t, \Phi_{t_0}^t(p)\right], \ \forall t \in [t_0, t_0 + T]$$

3. Integrate evolution of the mesochronic Jacobian

$$\frac{d}{dT}\nabla \tilde{f}_T(p) = \frac{1}{T}J_p(T) + J_p(T)\nabla \tilde{f}_T(p) - \frac{1}{T}\nabla \tilde{f}_T(p)$$

Direct finite difference method

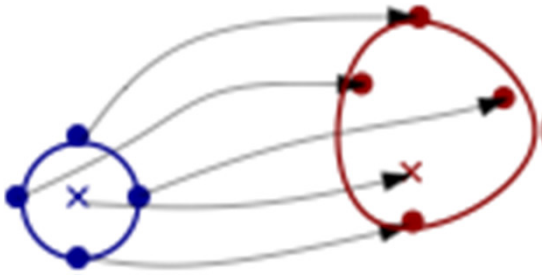

$$\partial_d \tilde{f}_T(p) = \frac{\tilde{f}_T(p + \delta\hat{p}_d) - \tilde{f}_T(p - \delta\hat{p}_d)}{2\delta}$$

For nonlinear flows, direct method is suspected to be inaccurate over longer integration times.

Test: Direct vs. 1st vs. 2nd order forward-evolution

ABC Flow, N=100 points, Incompressibility constraint: ideally, all points should be 0

Evaluate deviation from incompressibility condition: $\operatorname{tr} \nabla \tilde{f}_T + T \operatorname{tr} \operatorname{adj} \nabla \tilde{f}_T(p) + T^2 \det \nabla \tilde{f}_T(p) = 0$

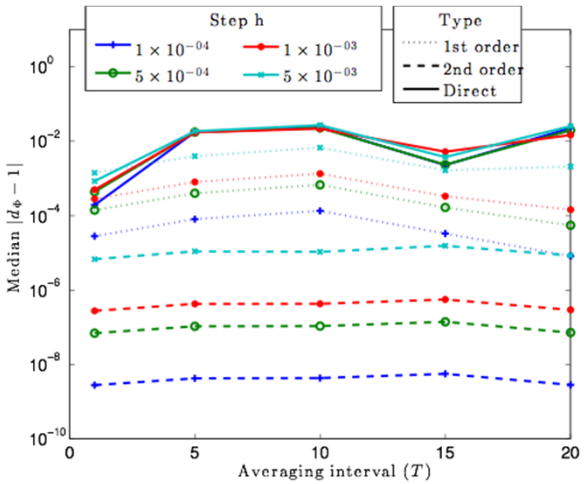

a) Median value of deviation

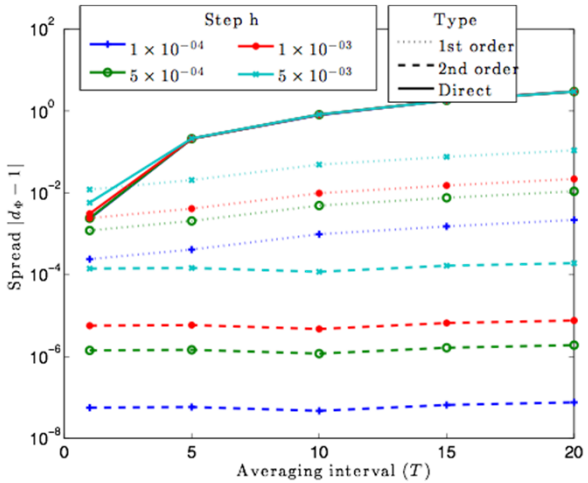

b) Difference betw. lower and upper 25%tile

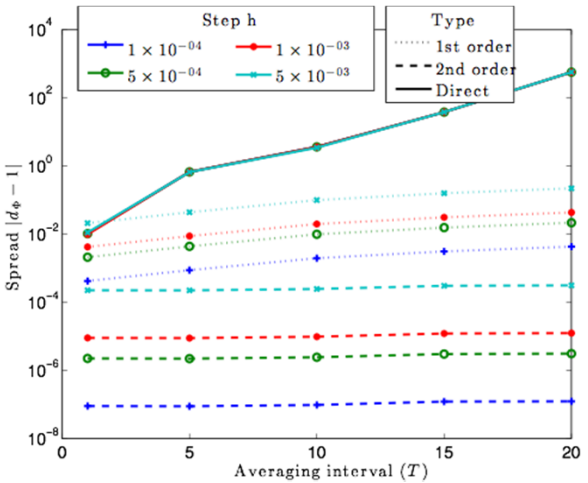

c) Difference betw. lower and upper 10%tile

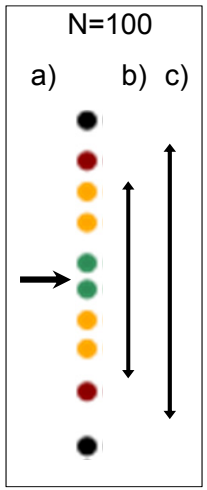

ABC Flow

$$\begin{bmatrix}\dot{x}\\ \dot{y}\\ \dot{z}\end{bmatrix} = \begin{bmatrix}A\sin z + C\cos y\\ B\sin x + A\cos z\\ C\sin y + B\cos x\end{bmatrix}$$

$$A^2 = 3,\ B^2 = 2,\ C^2 = 1$$

6 vortices, separated by **a chaotic region**

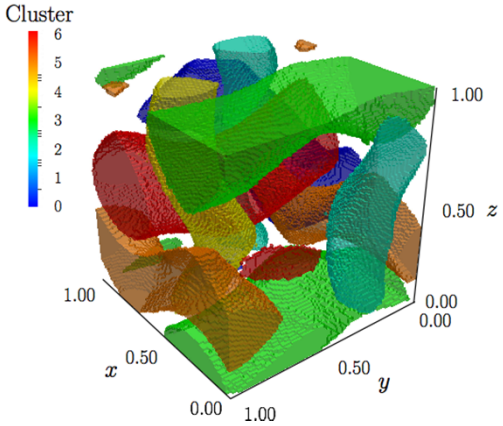

Top side of the 3d box (white is chaotic):

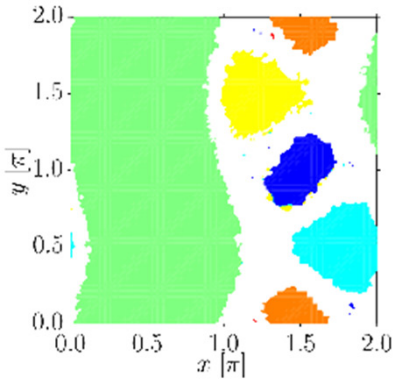

Timescales: vortex transport along unit cube takes cca. T = 2

Mesohyperbolicity (vortex boundaries in white)

$T = 1$

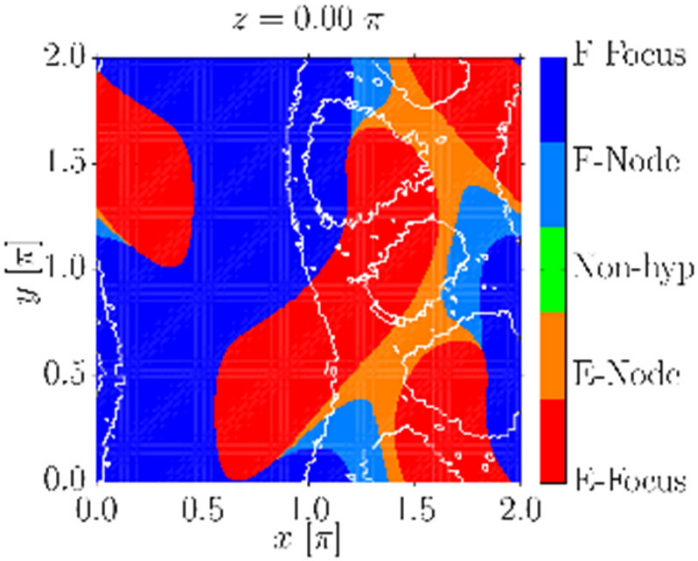

$T = 5$

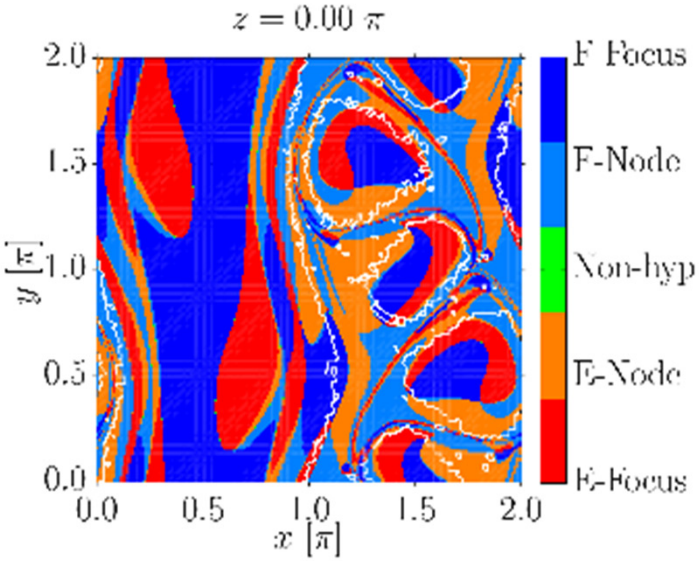

$T = 10$

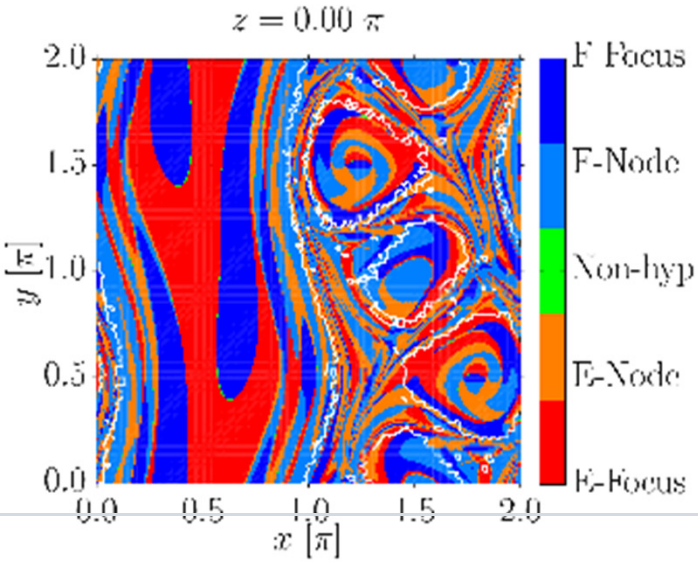

$T = 20$

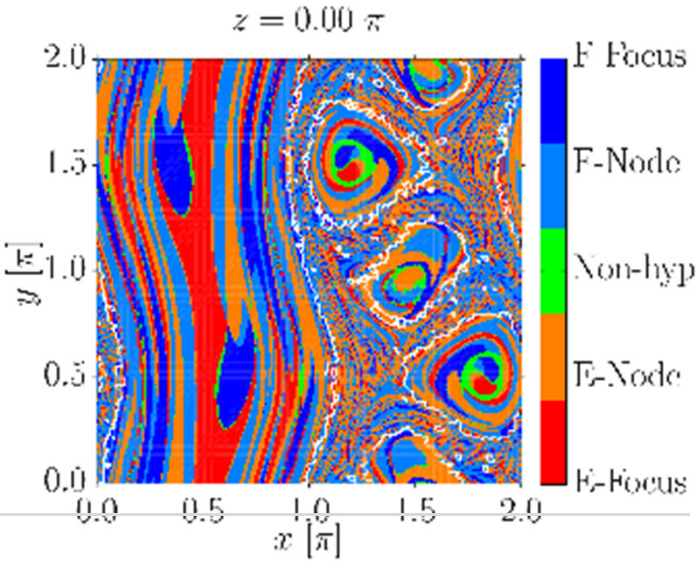

Space of quantifiers

$$x \in \mathbb{R}^3 \mapsto [\Delta(x), \Sigma(x), \mathcal{C}_-(x)]$$

Mapping 60 X 60 X 60 grid of initial conditions to the space of spectral quantifiers.

F-Focus

F-Node

E-Focus

E-Node

Non-hyp.

$T = 1$

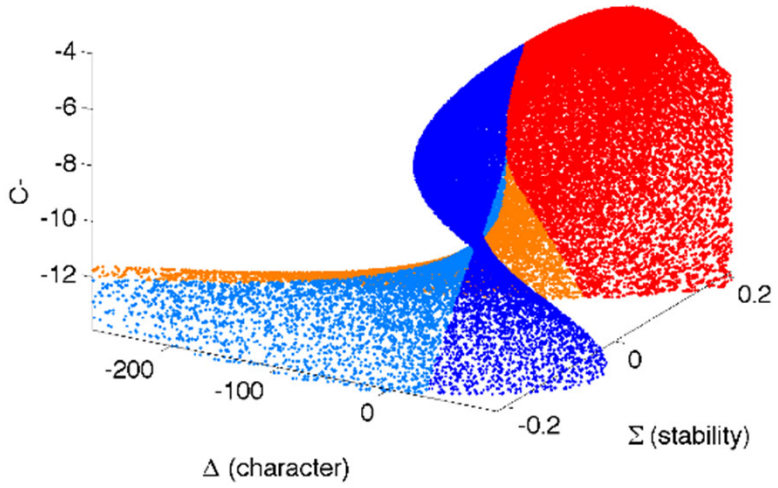

$T = 5$

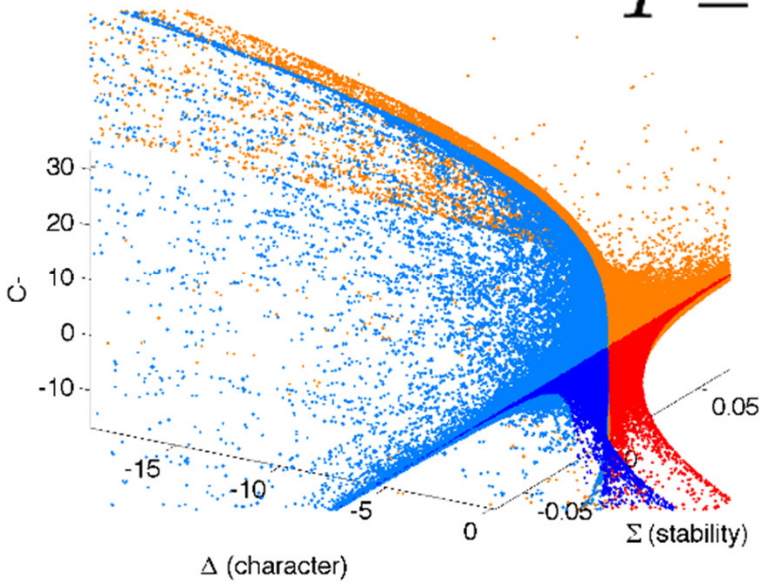

$T = 10$

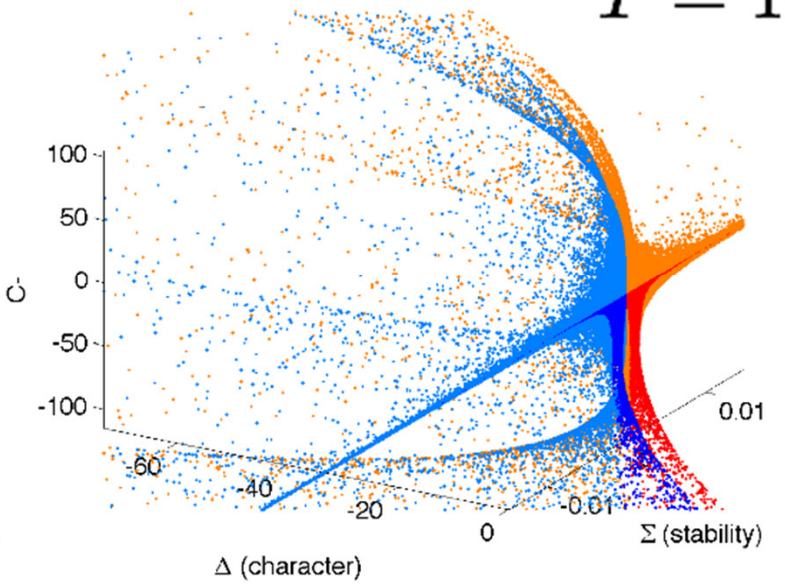

$T = 20$

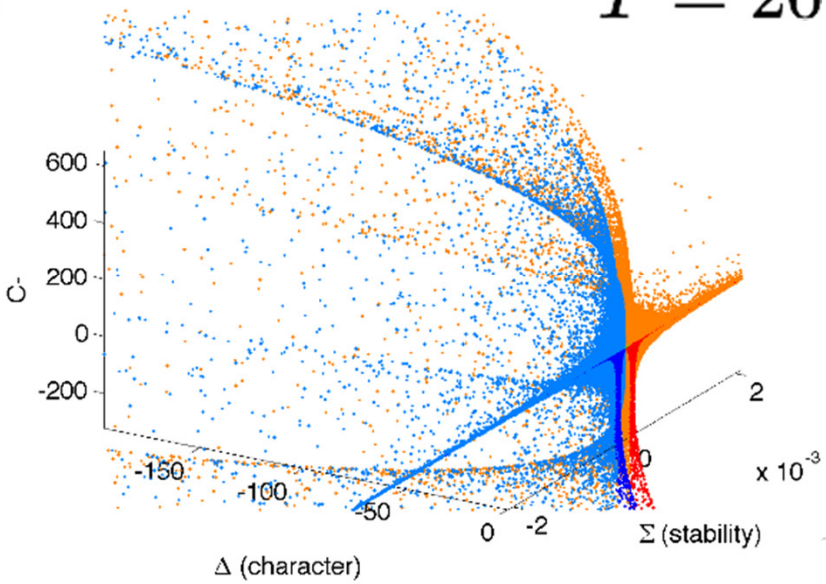

Boundary behavior

1. Instantaneous limit: $T \to 0$

$$\tilde{f}_T \xrightarrow{T \to 0} f$$

3D mesochronic criteria limit to 3D Okubo-Weiss (instantaneous hyperbolicity types).

2. Asymptotic limit: $T \to \infty$

$$\Delta = -4 d_{\tilde{f}}^4 T^6 + \mathcal{O}(T^5) < 0$$

$$\Sigma = -\frac{1}{3} T^{-3} + \frac{2 m_{\tilde{f}}}{9 d_{\tilde{f}}} T^{-4} + \mathcal{O}(T^{-5}) \to 0^-$$

Asymptotically, two possible types of behavior:
1)non-mesohyperbolic
2)(flattening) nodal mesohyperbolic

N F E

3. Degeneracy to a 2D flow (Mezic et al., Science, 2010)

$$\underline{f}(x,y,z) = \begin{bmatrix} g_1(x,y) \\ g_2(x,y) \\ 0 \end{bmatrix}$$

$$t_{\tilde{f}} + T m_{\tilde{f}} + T^2 d_{\tilde{f}} \equiv t_{\tilde{g}} + T d_{\tilde{g}}$$

2D incompressibility

$$\mathcal{C}_+ \equiv 0$$

$$\mathcal{C}_- \equiv 2(T^2 d_{\tilde{g}} - 4) = s \frac{\mathcal{D}_2}{d_{\tilde{g}}}$$

Degenerate flows are 3D non-hyperbolic

$$t_{\tilde{f}} \equiv t_{\tilde{g}}$$

$$m_{\tilde{f}} \equiv d_{\tilde{g}}$$

$$d_{\tilde{f}} \equiv 0$$

$$\Sigma \equiv 0$$

$$\Delta \equiv d_{\tilde{g}}^2 \boxed{\mathcal{D}_2}$$

2D mesohyperbolicity indicator

3D focal/nodal indicator limits to 2D mesohyperbolicity

Numerical results for a large averaging interval

$$T = 50$$

$$\varepsilon = 10^{-3}$$

$$\varepsilon = 10^{-4}$$

Numerical tolerance to mesohyperbolicity criterion:

$$|\mathcal{C}_+(x,T)| > \varepsilon$$

$$|\mathcal{C}_-(x,T)| > \varepsilon$$

Expected types of behavior:
1)non-mesohyperbolic
2)(Flattening) Nodal mesohyperbolic

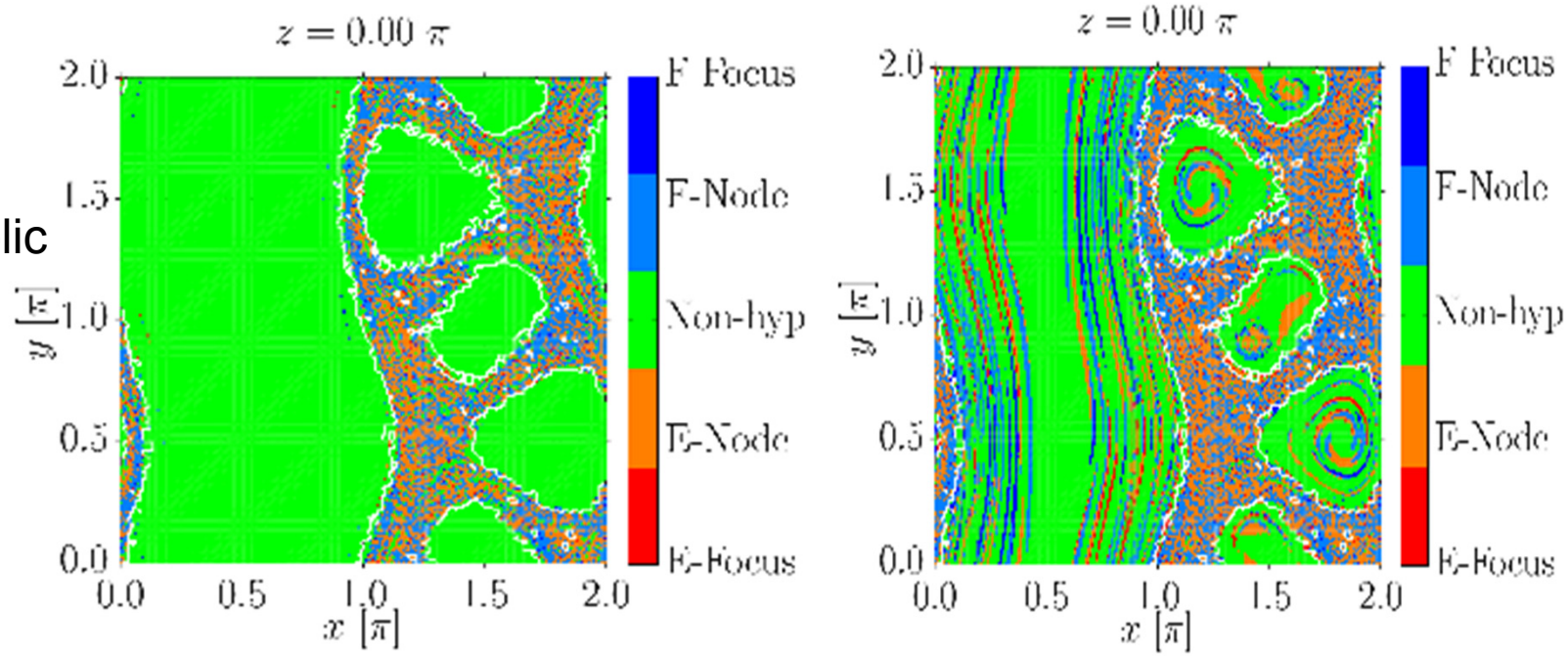

Mesohyperbolicity and optimal control

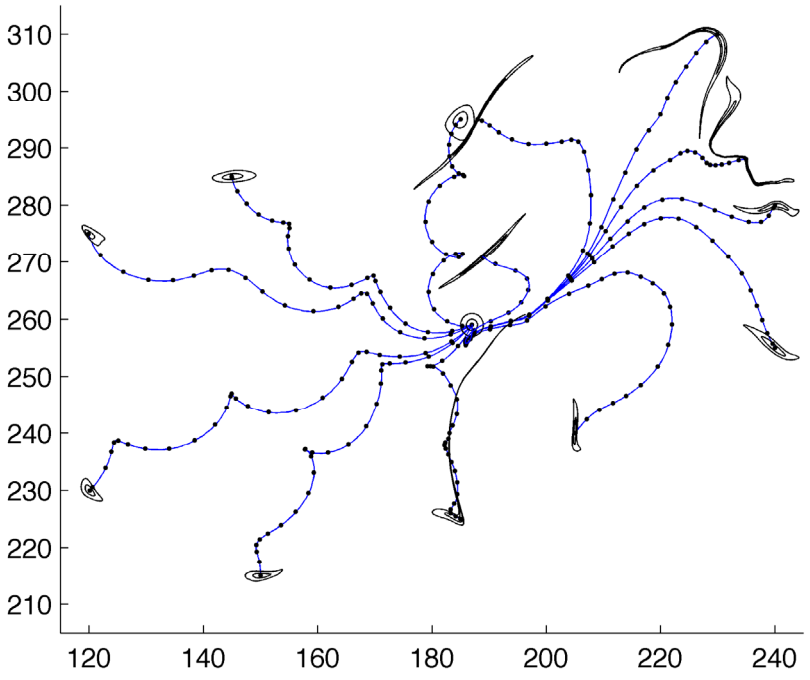

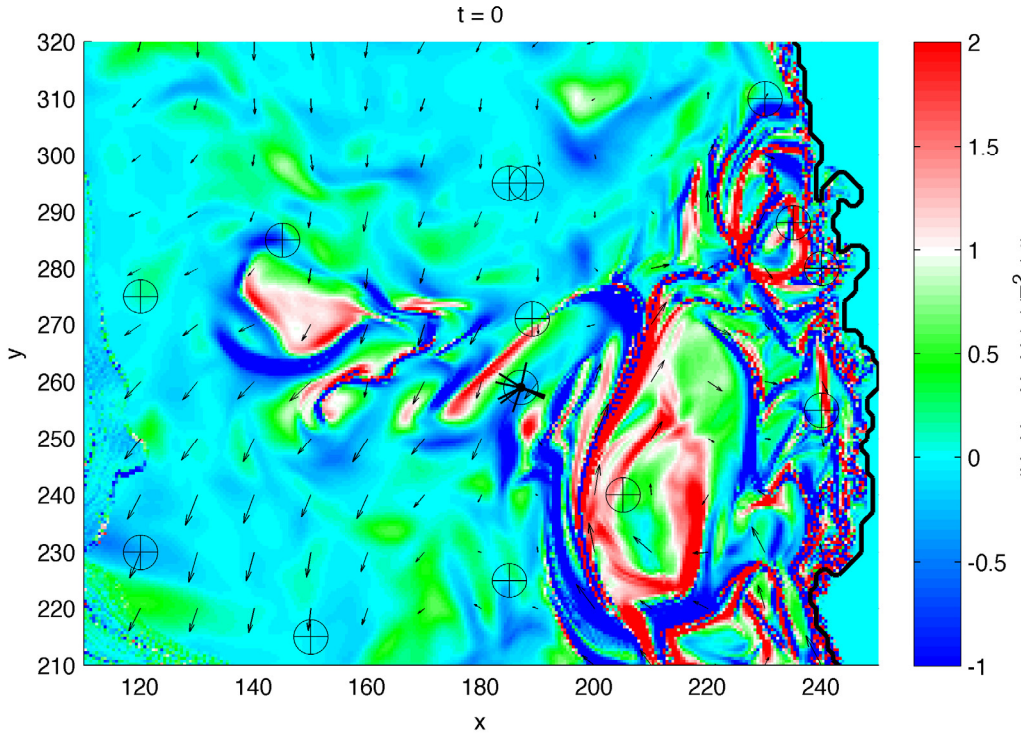

Mesohyperbolicity

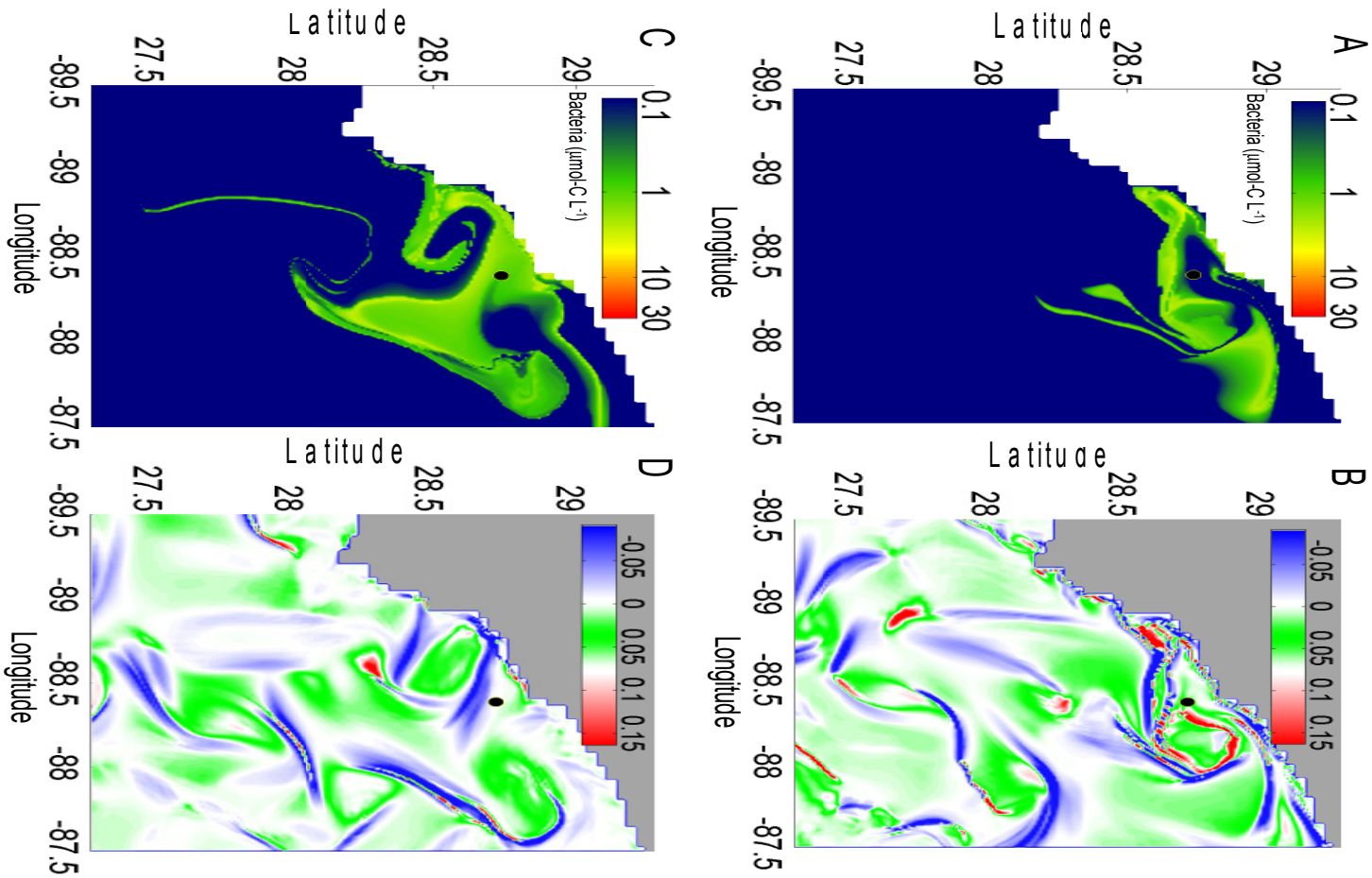

Flow Structures in 3D

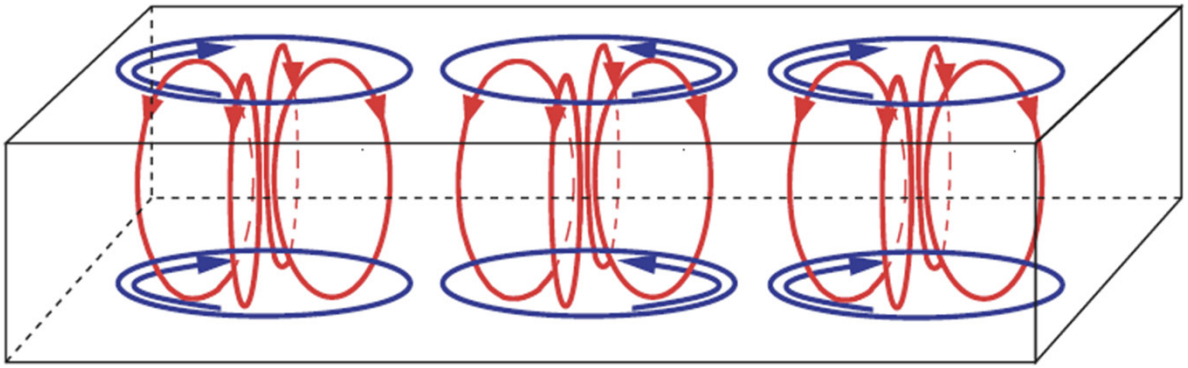

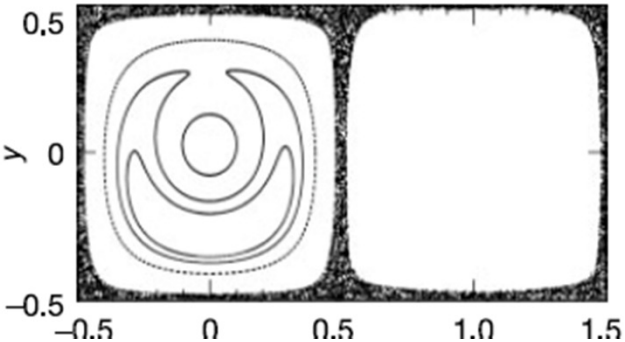

Mixing and transport dominated by spiral-node fixed pts and periodic orbits.

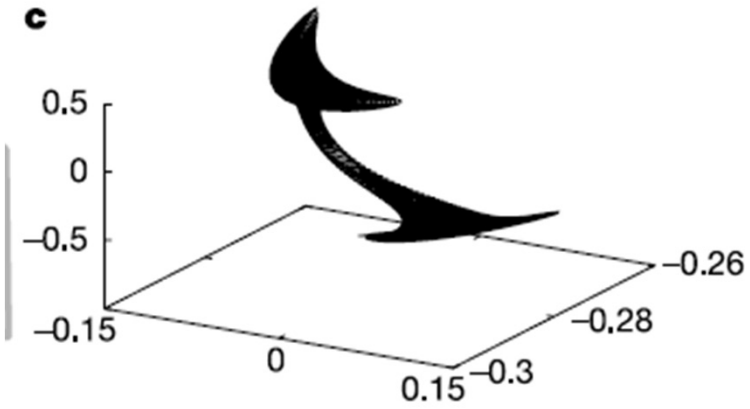

Solomon, I.M. Nature (2003)

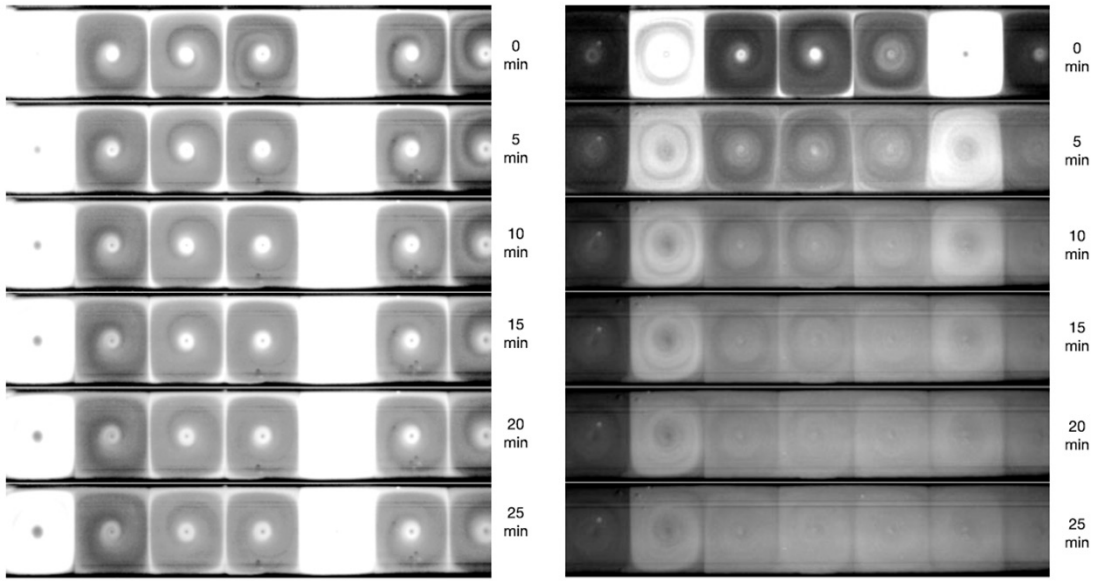

Koopman Mode Decomposition

I.M., Nonl.Dyn (2005)

$$v^{n+1}(x) = N(v^n(x), p)$$

$$v_x^n(m) = U_s^n v_x(m) = v^*(x) + \sum_{j=1}^{k} \lambda_j^n f_j(m) s_j(x) + \int_0^1 \exp(i2\pi\alpha)\, dE(\alpha) v(x,m)$$

Spatial modes

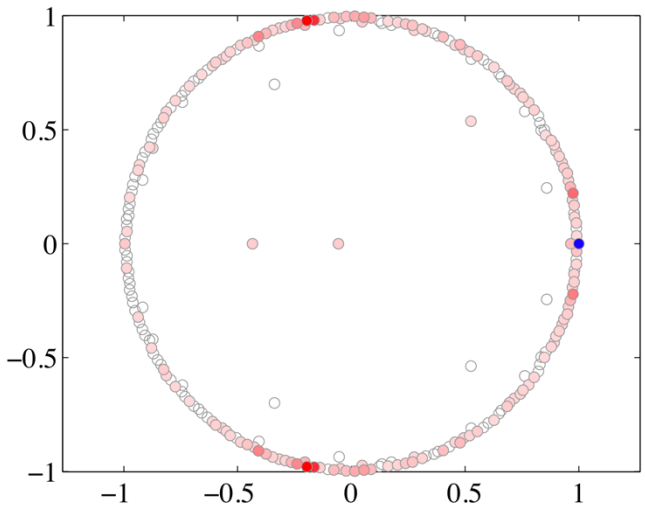

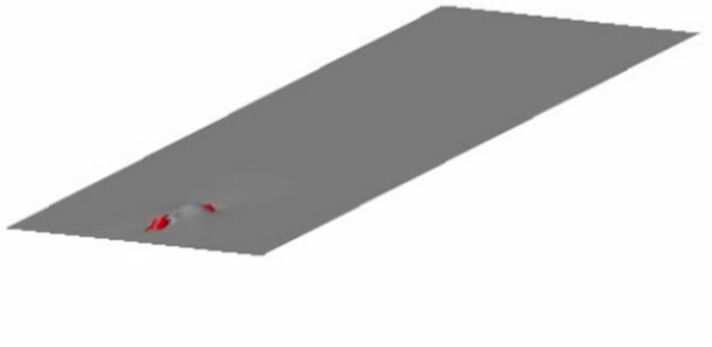

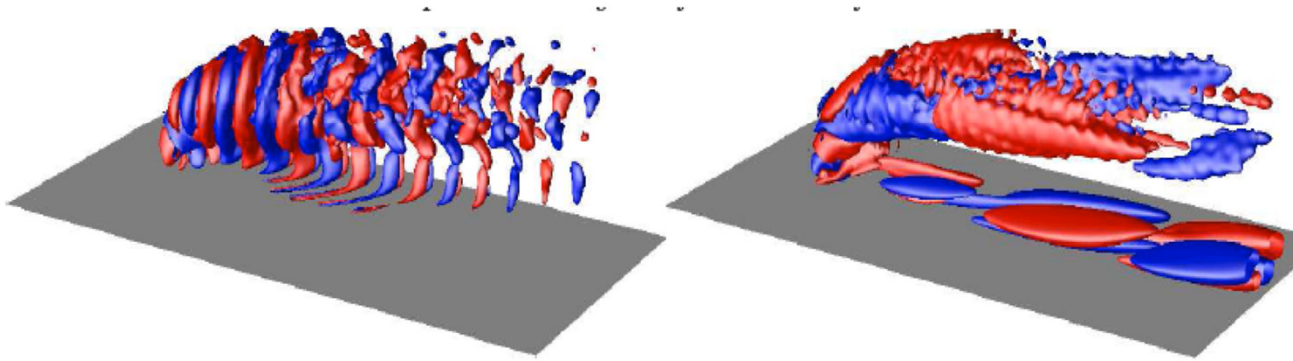

C.W. Rowley (Princeton), I. Mezic (UCSB),
S. Bagheri, P. Schlatter, and D.S. Henningson Royal Institute of Technology (KTH),
(Journal of Fluid Mechanics 2010)

I.M. ANN REV. FLUID MECH (201

Conclusions

- An experimental testbed fro 3D+1
-Extraction of flow features in 3-D time-independent and time-dependent flows.
-Mesohyperbolicity concept (introduced in Science paper) indicating robustness of computed features extended to 3D.
-An intuitive algorithm for control in 3D obtained using only flow concepts – simplifying optimal control computations.